Aerosol and Air Quality Research, 14: 45–63, 2014

ISSN: 1680-8584 print / 2071-1409 online
doi: 10.4209/aaqr.2013.07.0239

An Overview of Airborne Nanoparticle Filtration and Thermal Rebound Theory

Raheleh Givehchi[1], Zhongchao Tan[1,2*]

[1] *Department of Mechanical & Mechatronics Engineering, University of Waterloo, Ontario, Canada*
[2] *Waterloo Institute for Nanotechnology, University of Waterloo, Ontario, Canada*

ABSTRACT

This paper provides an overview of recent studies on the filtration of airborne nanoparticles. Classical filtration theory assumes that the efficiency of nanoparticle adhesion is at unity when nanoparticles strike a filter with a Brownian motion. However, it has been pointed out that small nanoparticles may have a sufficiently high impact velocity to rebound from the surface upon collision, a mechanism called thermal rebound. According to thermal rebound theory, the adhesion efficiency of nanoparticles decreases if their size is reduced. However, this phenomenon has not yet been clearly observed in experimental studies; there are still a number of uncertainties associated with the concept of thermal rebound, which is yet to be either proven or disproven. This review paper discusses the findings in the current literature related to thermal rebound theory.

***Keywords*:** Airborne nanoparticle; Filtration; Classical filtration theory; Thermal rebound.

INTRODUCTION

Nanoparticles are particles with at least one dimension less than 100 nm. Airborne nanoparticles are sometimes referred to as nanoaerosols and ultrafine particulate matters. Nanoaerosols comprise over 95% of particulate matters when the particle number distribution is considered (Whitby, 1978; Kittelson, 1998; Oberdörster *et al.*, 2005). This fact emphasises the importance of measuring nanoparticle number concentrations rather than their mass concentrations. Nanoparticles have a large surface area to volume ratio, which leads to a higher surface reactivity and has a significant effect on their properties (Paur *et al.*, 2011). Surface area is the most accepted characteristic for determining the toxicity of a nanoparticle, and is relied upon more than shape, and chemical composition (Oberdörster *et al.*, 2005).

Airborne nanoparticles can be generated from diverse sources but are produced primarily by the combustion (Donaldson *et al.*, 2005) and nanotechnology applications. The examples of nanoparticle combustion sources are transportation (Buseck and Adachi, 2008; Lim *et al.*, 2008; Lim *et al.*, 2009; Yin *et al.*, 2012), indoor fumes, smoking (Hofmann *et al.*, 2009; Van Dijk *et al.*, 2011), cooking (Wallace *et al.*, 2004; Torkmahalleh *et al.*, 2012), heating (Jung *et al.*, 2006), biomass, burning (Weimer *et al.*, 2009), etc. Nanoparticles are produced from other sources as well such as from polymers (Tsai *et al.*, 2008; Motzkus *et al.*, 2012), cleaning, laser printers (Wang *et al.*, 2011), photocopiers, agriculture (Buseck and Adachi, 2008), and welding. Nanoparticles are also generated from the applications of nanotechnology, in which their small size is essential, such as drug delivery, injections, inhalable medicines, and tracers (Allen and Cullis, 2004; Jawahar and Reddy, 2012; Tiwari *et al.*, 2012).

As the concentrations of airborne nanoparticles increase with the development of nanotechnology and other sources, concerns have arisen with respect to the potential negative impact on human health. Nanoparticles can cause adverse health effects due to the direct action of the particles or acting as carriers of toxic elements (Oberdörster *et al.*, 2005; McKenna *et al.*, 2008; Wang and Pui, 2011; Elsaesser and Howard, 2012). Because nanoparticles are not removed from the upper respiratory tract, they are inhaled into the deeper areas. Their rather high deposition (more than 90%) in the alveolar region or other respiratory tract regions leads to their subsequent entry into the blood stream (Oberdörster *et al.*, 1995; Castellano *et al.*, 2009; Marra *et al.*, 2010; Tsai *et al.*, 2012). The small size and large surface area of nanoparticles enable significant interaction with biological systems (Oberdörster *et al.*, 1995; Kreyling *et al.*, 2006; Roduner, 2006; Oberdörster *et al.*, 2007). As a result, nanoparticle exposure may cause numerous adverse health effects, such as ischemic heart disease, cardiovascular diseases, stroke, chronic bronchitis, asthma, and respiratory tract infections (Lin *et al.*, 2009; Mengersen *et al.*, 2011).

Among particle-removal technologies, filtration is the

* Corresponding author.
Tel.: 1-519-888-4567, ext. 38718
E-mail address: tanz@uwaterloo.ca

most common and simplest method of removing particulate matters from the air. Particles are deposited and captured upon collision with the surface of the filter, due to the adhesion energies between particles and a surface. Filtration has been used in diverse applications such as air cleaning, respiratory protection, nuclear and hazardous material processes, and clean rooms. Various types of filters are used in different applications for air cleaning, with the ones most commonly used being membrane and fibrous filters (Hinds, 1999).

The principles and fundamentals of airborne filtration have been validated with respect to micron particles; however, the mechanisms associated with the application of filters for airborne nanoparticles are still uncertain. For decades, nanoparticles were considered to be captured by a filter surface due to their Brownian motion. However, recent studies have pointed out that those small nanoparticles striking a filter surface could rebound if the amount of initial kinetic energy in the approaching particle surpasses that of the adhesion energy between the particle and the surface (Dahneke, 1971; Wang and Kasper, 1991). Nanoparticles are so small that they approach the size of molecules and they may behave like a gas molecule upon impaction. Wang and Kasper (1991) assumed that a nanoparticle strikes a surface with a mean impact velocity, based on the Maxwell-Boltzmann distribution, according to which the critical velocity of a nanoparticle is defined as that below which a particle can rebound from the surface. Consequently, filtration efficiency is thought to decrease for such small particles due to the thermal rebound. Uncertainties are still associated with the occurrence of thermal rebound in experimental and theoretical studies. A number of assumptions underline in thermal rebound theory: consideration of neutral particles, a Maxwell-Boltzmann distribution of the particle velocity, no energy loss, elastic impaction, normal impaction, and smooth surfaces. A question arises here if the consideration of these assumptions is applicable for airborne nanoparticles.

In the last few decades, there have been a great amount of publications that focused on nanoparticle filtration and thermal rebound. Advances in these areas of research deserve a systematic overview. This review paper provides an overview of nanoparticle filtration theory and the corresponding parameters that affect nanoparticle filtration efficiency; an experimentation of the analytical methods of developing thermal rebound theory for airborne nanoparticles, including a description of the effect of thermal rebound on filtration efficiency; and an in-depth discussion of the knowledge gaps related to nanoparticle filtration and thermal rebound. The conclusion to be derived from this analysis is that a great deal of uncertainty remains with respect to nanoparticle filtration.

NANOPARTICLE FILTRATION

The physical properties of nanoparticles and filters could affect the performance of air filters, so a better understanding of these parameters may help in the design of a high-performance filter for the efficient collection of nanoparticles. Particle filtration efficiency is calculated based on the efficiency of a single fiber. Several attempts have been made to calculate the single-fiber efficiency associated with a variety of particle deposition mechanisms of particles (Hinds, 1999). Among the developed methods, only a few can be used as a means of calculating single-fiber efficiency for nanoparticle removal. The following discussion is divided into two sections. Theoretical methods of calculating single-fiber efficiency for nanoparticles are first presented, followed by an examination of the effects of numerous parameters, such as humidity, particle shape, and fiber diameter, on nanoparticle filtration efficiency.

Calculation of Nanoparticle Filtration Efficiency

Classical theory to calculate the filtration efficiency (η) is expressed as a function of single fiber efficiency (E) (Hinds, 1999):

$$\eta = 1 - \exp\left(\frac{-4\alpha EL}{\pi d_f (1-\alpha)}\right) \tag{1}$$

where α is the solidity of the filter, L is the thickness of the filter, and d_f is the fiber diameter. This equation was obtained theoretically by correlation between single-fiber efficiency and total efficiency of a filter (Hinds, 1999). Single fiber efficiency is the fraction of particles deposited on a unit length of a single fiber which position is perpendicular to the air flow direction, without the existence of other fibers. The air flow field around an isolated fiber is different from that being surrounded by other fibers at a random position. The Kuwabara flow field accounts for the effect of flow interference in randomly distributed fibers to evaluate the single fiber efficiency (Kuwabara, 1959).

Single fiber efficiency is based on consideration of all the individual deposition mechanisms and overestimates the overall efficiency, because particles captured may be counted more than once. It is assumed that a particle is collected permanently by a fiber upon collision. With respect to nanoparticles, diffusion and interception are the most significant.

The primary mechanism whereby nanoparticles are deposited on surfaces is diffusion. The single fiber efficiency based on diffusion mechanism is a function of Peclet number (Pe), which defined as

$$Pe = \frac{d_f U}{D} \tag{2}$$

where U is the aerosol flow velocity, and D is the diffusion coefficient.The diffusion coefficient of particles with a low Reynolds number in air is the function of the particle diameter (d_p):

$$D = \frac{K_b T C_c}{3\pi\mu d_p} \tag{3}$$

where K_b is Boltzmann's constant $1.38 \times 10^{-23} J/K$, T is temperature, μ is air viscosity, and C_c is the Cunningham coefficient, which indicated the non-continuum interaction

between the particles and the carrier gas. Nanoparticles are small enough to approach the mean free path of a gas under normal conditions; the Cunningham coefficient is thus used as a means of including consideration of the slip condition in the gas flow:

$$C_C = 1 + Kn_P\left[1.257 + 0.4\exp\left(-\frac{1.1}{Kn_P}\right)\right] \quad (4)$$

where Kn_P is the particle Knudsen number that is calculated as the ratio of the mean free path of the gas (λ) and the particle diameter as follows:

$$Kn_P = 2\lambda/d_p \quad (5)$$

The Knudsen number is used for determining the validation of the flow continuity assumption in the Navier-Stokes equation. For nanoparticles, the continuum flow assumption fails and the flow becomes a free molecular, which means that each molecule travels between other molecules a number of times before collision with other molecules (Przekop and Gradoń, 2008).

The diffusion coefficient of a neutral nanoparticle in the range of 0.5 nm to 2 nm is given by (Leob, 1961)

$$D_n = \frac{0.815V_r}{3\pi\left(a + \frac{d_p}{2}\right)^2 N}\sqrt{1 + \frac{m}{M}} \quad (6)$$

where V_r is the mean velocity of the air (502 m/s at STP), a is the air molecule radius (0.185 nm), N is the concentration number of air molecules (2.45×10^{-25}/m^3 at STP), m is the molecular weight of the air (28.96 for air at STP), and M is the molecular weight of the particles. The molecular weight of the particles is much larger than that of the air molecules, so the square root term can be neglected (Ichitsubo *et al.*, 1996). For singly charged nanoparticles, Eq. (6) will be changed to (Ichitsubo *et al.*, 1996)

$$D = \frac{D_n}{1 + \frac{0.402e^2a^3}{4\left(a + \frac{d_p}{2}\right)^4 K_b T}} \quad (7)$$

The interception mechanism is more effective when particles approach a fiber within a one-particle radius distance. The efficiency is a function of interception parameter (R), which defined as

$$R = d_p/d_f \quad (8)$$

thus, capturing efficiency increases as the particle diameter increases and the fiber diameter decreases.

Single fiber efficiency based on consideration of Brownian diffusion and interception is given in Table 1.

A number of studies have been conducted in order to validate the models developed for calculating nanoparticle filtration efficiency as listed in Table 1. For example, Lee and Liu (1982) developed theoretical equations to express single-fiber efficiency, based on consideration of Brownian diffusion ($E_D = 2.6\left(\frac{1-\alpha}{Ku}\right)^{1/3} Pe^{-2/3}$) and interception ($E_R = (\frac{1-\alpha}{Ku})\frac{R^2}{1+R}$); however, these equations do not account the effect of gas slip. The experimental validation of the equations were based on consideration of a real filter with irregularities in fiber direction and non-uniformly distributed fibers, which showed that the numerical coefficients for diffusion and interception should be replaced by 1.6 and 0.6, respectively. Liu and Rubow (1990) later modified Lee and Liu (1982) equation by including consideration of the gas slip effect and correction factors of C_d and C_r for Brownian diffusion and interception, respectively. It was observed that the filtration efficiency of nanoparticles with a low Peclet number is greater than unity, so, in 1992, Payet *et al.* (1992) modified Liu and Rubow's (1990) diffusion efficiency equation by adding an additional correction factor ($C_{d'}$) to lower the efficiency value to less than unity. An experimental study was also employed as a means of validating the previous correction in particle size range from 80 nm to 400 nm (Payet *et al.*, 1992).

An experimental study by Podgórski *et al.* (2006), which employed sebacic acid-bis ester particles in the 10 nm to 500 nm range, showed that if the mean diameter of the fiber is considered, the theoretical equations proposed by Payet *et al.* (1992) for both diffusion and interception slightly overestimate the measured filtration efficiency data; however, the theoretical equations are in good agreement with experimental data if a resistance-equivalent fiber diameter is considered (Podgórski *et al.*, 2006). Steffens and Coury (2007) employed a high-porosity filter to collect NaCl particles in the range of 8.5 nm to 94.8 nm at aerosol flow velocities of 0.03 m/s to 0.25 m/s. The measured filtration efficiency showed that the equation predicted by Lee and Liu (1982) for both diffusion and interception mechanisms underestimated the experimental data, and that those predicted by Liu and Rubow (1990) overestimated the experimental data (Steffens and Coury, 2007). Wang *et al.* (2007) calculated filtration efficiency based on a Brownian diffusion of HF-type and HE-type filters with effective fiber diameters of 1.9 μm, 2.9 μm, 3.3 μm, and 4.9 μm and packing densities of 0.039, 0.047, 0.049, and 0.05, using silver particles in the range of 3 nm to 20 nm and NaCl particles in the range of 15 nm to 400 nm at aerosol flow rates of 5.3 cm/s, 10 cm/s, and 15 cm/s. The results showed that the filtration efficiency measured experimentally was in good agreement with the equation predicted by Stechkina (1966) if the Peclet number is larger than 100 and in good agreement with Krish and Stechkina's (1978) equation for a Peclet number in the order of unity. The authors developed an additional equation that is a function of a Peclet number ($E_D = 0.84Pe^{-0.43}$) and that is in good agreement for all Peclet numbers.

Table 1. Single fiber efficiency due to Brownian diffusion and interception.

Single fiber efficiency due to Brownian diffusion		
Pich, 1965	$E_D = 2.27Ku^{-1/3}Pe^{-2/3}(1 + 0.62Kn_f Pe^{1/3}Ku^{-1/3})$	$Ku = -0.5\ln\alpha - 0.75 - 0.25\alpha^2 + \alpha,\ Kn_f = \frac{2\lambda}{d_f}$
Stechkina, 1966	$E_D = 2.9Ku^{-1/3}Pe^{-2/3} + 0.624Pe^{-1}$	boundary layer analysis
Krish and Stechkina, 1978	$E_D = 3.2(Ku + \tau Kn_P)^{-1/2}(\tau Kn_P)^{1/2}Pe^{-1/23}$	Gas slip, if $\delta_1 = \left(\frac{2(Ku+\tau Kn)}{Pe}\right)^{1/3} < Kn$, δ_1 is the boundary layer length charectrstics, τ is a coefficient that is dependent on a gas-fiber interaction and it is assumed to be unity
Kirsch and Fuchs, 196	$E_D = 2.7Pe^{-2/3}$	No gas slip, $0.01 < \alpha < 0.15$
Lee and Liu, 1982	$E_D = 2.6\left(\frac{1-\alpha}{Ku}\right)^{1/3} Pe^{-2/3}$	No gas slip
Lee and Liu, 1982	$E_D = 1.6\left(\frac{1-\alpha}{Ku}\right)^{1/3} Pe^{-2/3}$	Fibers are not prependicular to the flow direction and are not uniformly distributed
Liu and Rubow, 1990	$E_D = 1.6\left(\frac{1-\alpha}{Ku}\right)^{1/3} Pe^{-2/3}C_d$	Gas slip, $C_d = 1 + 0.388Kn_f\left[\frac{(1-\alpha)Pe}{Ku}\right]^{1/3}$
Payet *et al*., 1992	$E_D = 1.6\left(\frac{1-\alpha}{Ku}\right)^{1/3} Pe^{-2/3}C_d C_{d'}$	Gas slip, $C_d = 1 + 0.388Kn_f\left[\frac{(1-\alpha)Pe}{Ku}\right]^{1/3}$ $C_{d'} = \left[1 + 1.6\left[\frac{1-\alpha}{Ku}\right]^{1/3} Pe^{-\frac{2}{3}}C_d\right]^{-1}$
Hinds, 1999	$E_D = 2Pe^{-2/3}$	No gas slip
Wang *et al.*, 2007	$E_D = 0.84Pe^{-0.43}$	Gas slip
Single fiber efficiency due to interception		
Krish and Stechkina, 1978	$E_R = \frac{1+R}{2Ku}[2\ln(1+R) - 1 + \alpha + \left(\frac{1}{1+R}\right)^2\left(1-\frac{\alpha}{2}\right) - \frac{\alpha}{2}(1+R)^2]$	No gas slip
Lee and Gieseke, 1980	$E_R = \left(\frac{1-\alpha}{Ku}\right)R^2(1+R)^{\frac{-2}{3(1-\alpha)}}$	No gas slip
Pich, 1966	$E_R = \frac{(1+R)^{-1} - (1+R) + 2(1+1.996Kn_f)(1+R)\ln(1+R)}{2(-0.75 - 0.5\ln\alpha) + 1.996Kn_f(-0.5 - \ln\alpha)}$	No gas slip
Lee and Liu 1982	$E_R = \left(\frac{1-\alpha}{Ku}\right)\frac{R^2}{1+R}$	No gas slip, $R < 0.2$, $\alpha < 0.5$
Lee and Liu, 1982	$E_R = 0.6\left(\frac{1-\alpha}{Ku}\right)\frac{R^2}{1+R}$	Fibers are not normal to the flow direction and are not uniform distributed
Liu and Rubow, 1990; Payet *et al*., 1992	$E_R = 0.6\left(\frac{1-\alpha}{Ku}\right)\frac{R^2}{1+R}C_r$	Gas slip, $C_r = 1 + \frac{1.996Kn_f}{R}$

Wang *et al.* (2008) employed four filters, with solidities of 0.134, 0.104, 0.059, and 0.034, and tested the penetration of silver particles in the range of 3 nm to 20 nm and that of NaCl particles in the range of 20 nm to 300 nm at face velocities up to 40 cm/s. The experimental data agrees well with the data calculated based on Brownian diffusion and interception predicted by Pich (1966) for particles larger than 20 nm (Wang *et al.*, 2008). Another experimental study, which employed neutral NaCl nanoparticles with diameters down to 10 nm at filtration velocities of 0.03 m/s to 0.5 m/s, demonstrated that the single-fiber efficiency predicted by Kirsch and Fuchs (1968) is in good agreement for wire screens, and that the efficiency predicted by Wang *et al.* (2007) is in good agreement for a real filter (Yamada *et al.*, 2011). Gómez *et al.* (2012) employed a mixed screen diffusion battery containing two aluminum screens surrounding a gold screen. The penetration of a sub-10 nm NaCl particle through the diffusion battery was measured, and the results showed that the single-fiber efficiency predicted by Kirsch and Fuchs (1968) agrees well with that

measured in the experiment, which was based on consideration of the equivalent fiber diameter of the diffusion battery (Gómez *et al.*, 2012). In conclusion, each theoretical study is best used in a specific situation related to the particular characteristics of the filter and particle, but none is accurate enough for use with a wide range of particle and filter parameters.

Another factor that influences filtration performance is the charge states of the particles (Chen and Huang, 1998). Most particles and filters may carry ions; however, the level of charges is so low that affect the filtration efficiency. It has been shown that filtration efficiency of small nanoparticles is much lower for uncharged particles than for highly charged ones, because of the lower charging efficiency the discrepancy between the removal of charged and uncharged particles decreases (Kim *et al.*, 2006) and the electrostatic forces may not play an important role to remove nanoparticles (Wang and Otani, 2013). Thus, the effective mechanisms for removing nanoparticles with low charged level are Brownian diffusion and interception that were completely discussed.

Another approach to the calculation of single fiber deposition efficiency is tracing the trajectory of a particle and determining the collision of the particle to the surface of a fiber. The Langevin equation is employed to describe the motion of nanoparticles, and Brownian dynamics algorithm is used to integrate the Langevin equation in order to calculate the single fiber efficiency. A detailed description of this algorithm is available in a number of earlier publications (e.g., Bałazy and Podgórski, 2007; Choi *et al.*, 2007; Podgórski and Bałazy, 2008; Sztuk *et al.*, 2012).

Based on classical filtration theory and Brownian dynamic algorithm, the removal efficiency for nanoparticles is significantly high and decreases with increased particle size due to lower levels of Brownian diffusion. However, studies indicate that small nanoparticles may rebound from the surface upon collision due to their high impact velocities, which causes a decrease in filtration efficiency. Thus, it is likely that another mechanism is associated with particle deposition, one that has adverse effects on small nanoparticles with respect to thermal rebound. This mechanism must be considered in any investigation of filtration efficiency. The effective parameters on filtration efficiency and advances in nanoparticle filtration will be discussed in the following section.

Advances in Nanoparticle Filtration Efficiency

The determination of the single-fiber efficiency of nanoparticles based on Brownian diffusion and interception is a function of the fiber diameter. Nanofibers with a diameter in the range of 100 nm to 1000 nm, are produced mainly through the use of electrospinning methods (Barhate and Ramakrishna, 2007). Filtration efficiency based on Brownian diffusion and interception increases with decreasing fiber diameter; however, the smaller the fiber diameter, the higher the pressure drop, a consideration that has led some researchers to experiment with multilayer filters, consisting of differing fiber diameters and densities in each layer (Podgórski *et al.*, 2006).

In recent years, a number of studies have been conducted with the goal of determining the filtration efficiency of nanofiber filters (Podgórski *et al.*, 2006; Qin and Wang, 2006; Yun *et al.*, 2007; Wang *et al.*, 2008; Hung and Leung, 2011). For example, Podgórski *et al.* (2006) employed fibrous filters that were composed of microfibers and nanofibers, with the mean fiber diameter varying from 0.74 μm to 1.41 μm, and that were produced by means of a melt-blown method for removing nanoparticles with diameters in the range of 10 nm to 500 nm in diameter. The use of such nanofiber filters resulted in greater efficiency than did the use of microfiber filters. For the collection of polydispersed particles containing nanoparticles, the authors recommended a triple-layer design filter, with dense micrometer-size fibers for support, porous nanofibers for the middle layer, and intermediate-size fibers for the front layer. Yun *et al.* (2007) carried out experiments with Polyacrylonitrile nanofibers with a mean fiber diameter of 0.27 μm to 0.4 μm produced by electrospinning in order to collect NaCl nanoparticles in the range of 10 nm to 80 nm and showed that nanoparticle penetration decreases with increased filter thickness; however, single-fiber efficiency and the quality factor are independent of filter thicknesses. Overall, studies have shown that due to Brownian diffusion and interception, nanofibers improve the efficiency of nanoparticle removal.

It has been shown that nanoparticle type (shape and material) could affect the filtration efficiency. Particle shape affects volume, surface area, and motion, with a consequent impact on the rate of filter cake formation, and filtration efficiency. Most particles are non-spherical, and their shape affects the drag force, settling velocity, and electrical mobility (Intra and Tippayawong, 2011). Studies show that cubic particles provide lower particle removal efficiency than do aerodynamically similar spheres. The contact areas following collisions between the filter surface and spherical particles travelling in divergent directions are the same; however, this area may be different for other particle shapes, which alter particle collection efficiency (Boskovic *et al.*, 2005). Spherical particles may either slide or roll upon collision; however, cubic particles could either slide or tumble, increasing the probability of detachment from the surface (Boskovic *et al.*, 2005). An experimental study has determined the effect of particle shape on filtration efficiency. At a filtration velocity of 5 cm/s to 20 cm/s, three particle shapes in the range of 50 nm to 300 nm in diameter were considered: spherical PSL, perfect MgO cubes, and transitional NaCl cubes with rounded corners particles. The finding showed that spherical particles result in greater removal efficiency, followed by NaCl and MgO. The rounded corners or sharp edge of the NaCl particles cause them to roll or tumble, respectively, upon contact with the surface (Boskovic *et al.*, 2008). Particle shape is thus a significant factor that affects filtration characteristics, dust cake formation, and filtration efficiency (Nazarboland *et al.*, 2007). The particle material could affect the efficiency of the filter because of differences in shape, densities, hardness, electrostatic forces, and chemical reactions. Numerous studies have been conducted with respect to the effect of different kinds of particle materials: sodium chloride (Bałazy *et al.*,

2004; Heim *et al.*, 2005), diethylhexyl phthalate (DEHP) (Bałazy *et al.*, 2004; Japuntich *et al.*, 2007), silver (Kim *et al.*, 2007), graphite (Golanski *et al.*, 2010), and titanium dioxide (Golanski *et al.*, 2010). However, these studies have revealed no obvious linked between the type of aerosol and filtration efficiency, and the removal efficiency discrepancy attributes to the difference in particle shape.

It is observed that increasing level of humidity increases removal efficiency of the filter for micron size particles (Brown, 1993; Miguel, 2003); however, this application for nanosized particles is still in doubt. Kim *et al.* (2006) tested the filtration efficiency for sub-100 nm neutralized NaCl particles at a face velocity of 2.5 cm/s and at different humidity conditions: 0.04%, 1.22%, and 92%. The results showed for sub-100 nm particles, that filtration efficiency is independent of relative humidity, because capillary force has no effect on nanoparticles adhesion (Kim *et al.*, 2006). Unfortunately, no more researchers determined the effect of humidity on nanoparticle filtration efficiency.

THERMAL REBOUND

In the past, it was considered that airborne nanoparticles were captured by a surface due to Brownian diffusion; however, Wang and Kasper (1991) suggested the possibility of a thermal rebound theory for particles smaller than 10 nm. When a particle hits the surface, its initial kinetic energy is transformed to elastic deformation and is lost as plastic deformation or heat. If all of the initial kinetic energy is consumed, the particle stops and sticks to the surface; otherwise, if the energy stored as elastic deformation is high enough to overcome the adhesion energy, the particle rebounds from the surface. The adhesion of a particle to a surface is thus related to its impact velocity. For impact velocities lower than the critical velocity, particles stick to the surface, and at impact velocities higher than the critical level, they rebound from the surface. The following section is divided into analytical work and experimental work regarding thermal rebound of nanoparticles.

Analytical Work

Wang and Kasper (1991) developed a thermal rebound theory based on consideration of impact velocity and critical velocity of nanoparticles. The particle impact velocity was characterized by thermal velocity, which is based on the Maxwell-Boltzmann distribution in a Brownian motion. A Maxwell-Boltzmann distribution describes the speed of molecules in an ideal gas flow characterized by thermal velocity, in which the molecules move randomly, rapidly, and freely without any interaction with other molecules; however, brief elastic collisions may occurs (Mandl, 1988). The probability density function of molecule speed in a gas flow is expressed according to a Maxwell-Boltzmann distribution as

$$f(v) = 4\pi v^2 \sqrt{\left(\frac{m}{2\pi K_b T}\right)^3} exp(-\frac{mv^2}{2K_b T}) \tag{9}$$

where $f(v)$ is the probability density function, v is the velocity of the molecule, and m is the mass of the molecule. The mean impact velocity of the molecule is

$$V_{im} = \sqrt{\frac{8K_b T}{\pi m}} \tag{10}$$

replacing the molecular mass with the particle mass based on consideration of particle density (ρ_P) and diameter (d_P), the mean impact velocity of a particle is defined as follows (Wang and Kasper, 1991):

$$V_{im} = \left[\frac{48K_b T}{\pi^2 \rho_P d_P^3}\right]^{1/2} \tag{11}$$

A Maxwell-Boltzmann distribution determines the speed of gas molecules that are moving freely in the flow; however, particles may not move freely without interaction with other particles. In reality, the particle resistance in a gas flow and the viscosity of the flow cause decreases in particle speed and have not been considered in literatures. Nanoparticles could agglomerate and changes in particle size and particle number concentration that may alter their speed distribution. Thus, a Maxwell-Boltzmann distribution might not be the best approach for the calculation of the thermal impact velocity of nanoparticles, and it is one of the analytical sources of error for thermal rebound theory.

The particle critical velocity is defined based on the conservation of energy, in which, the summation of the kinetic and potential energy of a particle prior to and after a collision remains the same (Dahneke, 1971):

$$KE_{nr} + E_{nr} = (KE_{ni} + E_{ni}) \cdot e^2 \tag{12}$$

where *nr* and *ni* refer to the rebound particle and the impact particle, respectively, and e is the coefficient of restitution. KE and E indicate the kinetic energy and the potential energy of a particle, respectively. When consideration of the particle mass and velocity is included, the equation changes to

$$\frac{v_{nr}}{v_{ni}} = \left(e^2 - \frac{E_{nr} - E_{ni} \cdot e^2}{mv_{ni}^2 / 2}\right)^{1/2} \tag{13}$$

If v_{nr} approaches zero, the particle will be captured, and the critical velocity is thus defined as

$$V_{cr} = \left[\frac{2}{me^2}\left(E_{nr} - E_{ni} \cdot e^2\right)\right]^{1/2} \tag{14}$$

Two situations of the equation above may exist:

$$E_{nr} = E_{ni} = E \rightarrow V_{cr} = \left[\frac{2E\left(1-e^2\right)}{me^2}\right]^{1/2} \tag{15}$$

$$E_{nr} >> E_{ni} \rightarrow V_{cr} = \left[\frac{2E_{nr}}{me^2}\right]^{1/2} \quad (16)$$

Wang and Kasper (1991) employed Eq. (16) to calculate the critical velocity, above which thermal rebound occurs. It is assumed that the potential energy of the particle after impaction is significantly greater than the potential energy before impaction and that is equal to the particle-surface adhesion energy. However, nanoparticles may have the negligible potential energy before and after impaction because of their small size and the assumption might be wrong.

Particle impaction is characterized by a coefficient of restitution that is the ratio of the rebound velocity to the impact velocity. Models have been developed for predicting the coefficient of restitution (Tabor 1948; Wu *et al*., 2003; Stevens and Hrenya, 2005), based on which the amount of the energy loss can be estimated. Energy loss could occur during plastic deformation, adhesion, friction and vibration. A number of researchers have predicted the energy loss to elastic deformation when a particle strikes a surface and have shown that a small fraction of the kinetic energy is lost (Hunter, 1957; Hutchings, 2001). The coefficient of restitution for impaction of different type of micron particles to a hard smooth surface was in the range of 0.73 to 0.84 (Wall *et al.*, 1990). In previous theoretical studies of thermal rebound, the coefficient of restitution was assumed to be near unity for small particles (Dahneke, 1971; Wang and Kasper, 1991; Mouret *et al.*, 2011). However, for nanometer-sized particles the coefficient of restitution may not be unity and the absolute value is unknown (Ayesh *et al.*, 2010). Studies show that the coefficient of restitution is dependent on the impact velocity as well as the material and surface of a nanoparticle (Sato *et al.*, 2007; Ayesh *et al.*, 2010; Jung *et al.*, 2010; Rennecke and Weber, 2013b). The coefficient of restitution is small for impact velocities close to the critical velocity (Rennecke and Weber, 2013b), which leads to small rebound velocities. The molecular dynamic simulation for collision of nanoparticles at room temperature showed that nanoparticles in the range of 0.5 to 2 nm did not rebound from the surface due to their significant energy loss (Sato *et al.*, 2007). The coefficient of restitution is also dependent on the mechanical properties and hardness of nanoparticles and surface. The coefficient of restitution is smaller for impaction between a harder particle and a softer surface, as stored energy transfers to lost energy due to the difference between the mechanical properties of the nanoparticle and the surface (Sato *et al.*, 2007). Therefore, the coefficient of restitution for a nanoparticle has a small value that should be taken into account in thermal rebound studies.

A variety of theories have been developed for calculating the adhesion energy between a particle and a surface based on elastic or plastic impaction. Common elastic adhesion energy models are the Bradley-Hamaker (BH), Hertz, Johnson-Kendall- Roberts (JKR), and Derjaguin-Muller-Toporov (DMT) models, and plastic adhesion energy is represented by the Maugis-Pollock (MP) model as described in the following subsections.

BH Elastic Adhesion Energy

The BH theory is used to consider van der Waals interactions between two rigid spheres (Bradley, 1932). The BH model assumes a point of contact between bodies due to van der Waals forces and fails to consider the adhesion force resulting from the impaction. The interaction energy between spherical particles with a diameter of d_p and a flat surface is given by

$$E_{ad} = \frac{A_H}{12}\left[\frac{d_p}{Z_0} + \frac{d_p}{d_p + Z_0} + 2\ln\left(\frac{Z_0}{d_p + Z_0}\right)\right] \quad (17)$$

where A_H is the Hamaker constant between a particle and a surface, which are available in literatures (Tsai *et al.*, 1991), and Z_0 is the equilibrium distance between bodies (0.4 nm). The Hamaker constant is typically in the order of 10^{-19} to 0^{-20} joules. As the particle approaches the surface, the adhesion energy is given as

$$E_{ad} = \frac{A_H d_p}{12 Z_0} Z_0 \rightarrow 0 \quad (18)$$

Eq. (18) is valid only for large particles and it does not apply to nanoparticles. The Hamaker constant between the particle and the surface is given as

$$A_H = \sqrt{A_{H1} A_{H2}} \quad (19)$$

where A_{H1} and A_{H2} are the Hamaker constants of a particle and a surface, respectively.

Hertz Elastic Adhesion Energy

Another model of the non-adhesive contact of a sphere on a plane with no surface forces was described by Hertz (1882), whose theory is based on a frictionless interface between the bodies, a flat surface, small strains in the elastic limit, a hemispherical pressure distribution in the contact area of the bodies, no pressure outside the contact area, and consideration of an elastic half-space solid. The contact radius between bodies (a), the adhesion energy E_{ad}, and the deformation height (δ) in the Hertz model are given by

$$a^3 = FR^*/K^* \quad (20)$$

$$E_{ad} = \Delta\gamma\pi a^2 \quad (21)$$

$$\delta = a^2/R^* \quad (22)$$

where F is the external force, K^* is the composite Young's modulus, and R^* is the characteristic radius of two bodies with diameters of d_p and d_s:

$$K^* = \frac{4}{3\pi}\left(K_P + K_S\right)^{-1} \quad (23)$$

$$K_i = \frac{1-\nu_i^2}{\pi E_i} \tag{24}$$

$$R^* = \left(\frac{2}{d_p} + \frac{2}{d_s}\right)^{-1} \tag{25}$$

where E_i is the elastic Young's modulus, ν_i is the Poisson ratio of the material, and K_i is the mechanical constant of material.

According to this theory, any surface interactions such as van der Waals forces and adhesive interactions between bodies are not considered, and the application is restricted to small amounts of deformation and linear elasticity. The presence of an adhesion force causes the contact radius to be larger than that predicted by the Hertz model, and in the absence of a load, the contact radius is not zero, so a pull-off force is required in order to separate the particle from the surface.

JKR Elastic Adhesion Energy

Based on the Hertz theory (1896), Johnson, Kendall, and Roberts (1971) developed the JKR model for considering the surface adhesion energy between elastic solids inside the contact area. The contact area between solids is significantly larger than that predicted by the Hertz model even at lower loads and is likely to be a constant contact diameter when the load approaches zero; however, the contact radius is smaller than that in plastic deformation models. The JKR model considers the effect of adhesion energy and contact pressure inside the contact area. The contact radius between bodies and the adhesion energy are therefore respectively given by the following two equations:

$$a^3 = \frac{R^*}{K^*}\left(F + 3\Delta\gamma\pi R^* + \sqrt{6\Delta\gamma\pi R^* F + \left(3\Delta\gamma\pi R^*\right)^2}\right) \tag{26}$$

$$E_{ad} = \Delta\gamma\pi a^2 \tag{27}$$

and the contact radius at zero applied force is changed to

$$a = \left(\frac{6\Delta\gamma\pi R^{*2}}{K^*}\right)^{1/3} \tag{28}$$

where $\Delta\gamma$ is the surface adhesive energy per unit contact area that accounts for the surface energy of both materials per contact area:

$$\Delta\gamma = \gamma_1 + \gamma_2 - \gamma_{12} \tag{29}$$

where γ_1 and γ_2 are the adhesion components of surfaces that are equal for identical materials, and γ_{12} is the interaction adhesion energy between bodies, which is zero for smooth surfaces. Considering that the surface adhesive energy per unit area results from van der Waals forces, the adhesion energy can be presented as a Hamaker constant, as follows (Derjaguin *et al*., 1975; Xu and Willeke, 1993):

$$\Delta\gamma = \frac{A_H}{12\pi Z_0^2} \tag{30}$$

It has been shown that the pull-off force is independent of the elastic and Young's modulus and is given as

$$F_{pull-off} = -\frac{3}{2}\Delta\gamma\pi R^* \tag{31}$$

The contact radius in the JKR adhesion model can be changed to that of the Hertz model ($a^3 = FR^*/K$) if the surface adhesive energy is neglected ($\Delta\gamma = 0$).

DMT Elastic Adhesion Energy

Derjaguin, Muller, and Toporov (1975) developed another adhesion model known as the DMT model, which included the consideration of the van der Waals contact interactions between solids inside the contact area. They found that the repulsive interaction forces between bodies cause deformation of the particles (Derjaguin *et al.*, 1975). The effectiveness of the model has been proven for smaller and stiffer contact solids (Rahmat *et al.*, 2012). However, the main defect in this theory is that it neglects deformations outside the contact area (Maugis, 2000). The contact radius (a), deformation depth (δ), and pull-off force are respectively given by

$$a^3 = \frac{R^*}{K^*}(F + 2\Delta\gamma\pi R^*) \tag{32}$$

$$\delta = \frac{a^2}{R^*} \tag{33}$$

$$F_{pull\text{-}off} = 2\Delta\gamma\pi R^* \tag{34}$$

In Eq. (32), at zero applied force, the contact radius changes to

$$a^3 = \left(\frac{2\Delta\gamma\pi R^{*2}}{K^*}\right)^{1/3} \tag{35}$$

The adhesion energy (E_{ad}) between a particle and a surface is given as

$$E_{ad} = \Delta\gamma\pi a^2 \tag{36}$$

Table 2 summarizes the BH, JKR, and DMT elastic models and their assumptions. As can be observed, the pull-off force in the JKR model differs from that according to the DMT or BH models because these models are used on two different sides of a Tabor parameter spectrum (Tabor, 1977).

Tabor Coefficient

The Tabor coefficient can provide an explanation of the contradictions among the JKR, DMT, and BH elastic

Table 2. Contact mechanical models.

Model	Explanation	Pull-off force
JKR	Fully elastic, adhesion force	$P = 3/2\Delta\gamma\pi R^*$
BH	Fully elastic, van der Waals	$P = 2\Delta\gamma\pi R^*$
DMT	Fully elastic, adhesion force and van der Waals	$P = 2\Delta\gamma\pi R^*$

models (Tabor, 1977). The Tabor coefficient (μ) is the ratio of the elastic displacement of surfaces to the effective range of surface forces at the pull-off point, and it indicates which model is applicable:

$$\mu = \frac{\left(R^*\right)^{\frac{1}{3}}\left(\Delta\gamma\right)^{\frac{2}{3}}}{Z_0\left(E^*\right)^{\frac{2}{3}}} \tag{37}$$

where E^* is reduced Young's modulus for a particle and a surface:

$$E^* = \frac{3}{4}K^* = \frac{1}{\pi\left(K_P + K_S\right)} \tag{38}$$

Accordingly, for small value of Tabor parameter, BH and DMT models, and for large Tabor parameter, JKR model is more applicable. As shown in Fig. 1, the normalized pressure load ($\bar{P} = P/\pi wR$, where P is pull-off force) varies continuously from 2, in the DMT model (for $\lambda < 0.1$, where λ is the elasticity parameter defined as $\lambda = 1.6\,\mu$), to 3/2, in the JKR model (for $\lambda > 5$) (Greenwood, 1997; Johnson and Greenwood, 1997; Muller *et al.*, 1980; Tsai *et al.*, 1991). The DMT theory is used for hard materials, small radii, and low adhesion energies, and JKR model is applied for soft material, large radii, compliant spheres, and large adhesion energy (Maugis, 2000).

Johnson and Greenwood presented the adhesion map and suitable model by dividing $\bar{P} - \lambda$ diagram into regimes based on elasticity parameter that correspond to different elastic models as shown in Fig. 2 (Johnson and Greenwood, 1997).

MP Plastic Adhesion Energy

The previous models considered elastic contact between materials; however, Krupp (1967) suggested that plastic deformation could occur in the inner circular region, and elastic deformation could occur in the outer one. The Maugis-Pollock (MP) plastic model is used for calculating the particle adhesion energy upon plastic collision (Maugis and Pollock, 1984). The contact area between bodies is determined through consideration of the hardness of the deformed material (H) and the specific adhesion energy ($\Delta\gamma$). The relation between the contact radius and the external force is given as

$$F = \pi a^2 H - 2\pi\Delta\gamma R^* \tag{39}$$

where F is the external load, and H is the hardness of the deformed solid. After complete plastic deformation, the mean pressure becomes constant, and the hardness can be calculated as $H = 3Y$, where Y is the elastic limit, or yield stress. When the external force is zero, the contact radius and the adhesion energy are given by

$$a = \left(\frac{2\Delta\gamma R^*}{H}\right)^{1/2} \tag{40}$$

$$E_{ad} = \Delta\gamma\pi a^2 \tag{41}$$

The particle critical velocity in a plastic regime can thus be calculated and compared with the impact velocity of particles with a wide range of diameters in order to determine the probability of the occurrence of thermal rebound.

The elastic yield velocity is used to define the plastic and elastic regimes of particle deformation upon collision, and the impaction changes continuously from elastic to

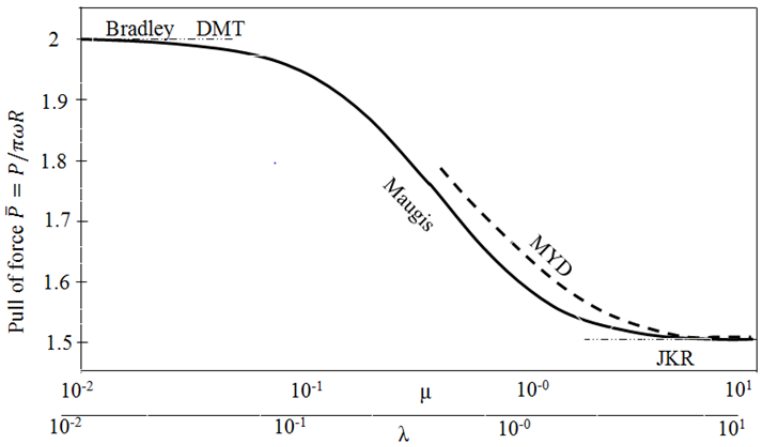

Fig. 1. Variations in the normalized pressure load by elasticity parameter (λ) or the Tabor parameter (μ); courtesy of (Johnson and Greenwood, 1997).

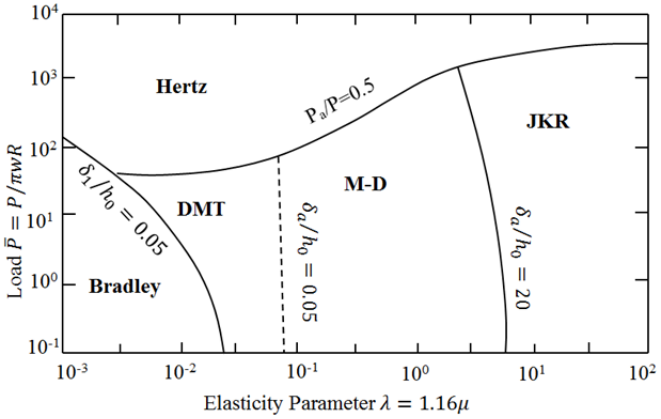

Fig. 2. Adhesion map: courtesy of (Johnson and Greenwood, 1997).

plastic deformation because of the increases of the impaction velocity. The elastic yield velocity can be described as follows (Xu and Willeke, 1993):

$$v_y = \left(\frac{2\pi}{3K^*}\right)^2 \left(\frac{2}{5\rho_P}\right)^{1/2} Y^{5/2} \tag{42}$$

The elastic limiting velocity is dependent on the density, elastic strain limit and mechanical constant of the particle as well as the surface material with different mechanical constant. For different particles and filters, the elastic and plastic impaction regimes also differ. And this should be taken into consideration in the studies of thermal rebound theory.

Wang and Kasper (1991) employed BH (Eq. (18) and JKR models (Eqs. (27) and (28)) for calculating the adhesion energy between a spherical particle and a surface. The BH theory considers the van der Waals interactions and the point of contact between the particle and the surface; however, the JKR theory takes into account the adhesion energy and the contact area between the particle and the surface. Due to the relatively minor differences between these theories, the JKR theory, which includes consideration of the finite contact area, was employed in Wang and Kasper's research for the calculation of the adhesion energy of the particle and the surface. As a result the respective calculation of adhesion energy and critical velocity based on consideration of JKR theory are as follows:

$$E_{ad} = \Delta\gamma\pi a^2 = \left[\frac{81}{64}\pi^7 d_P^4 \Delta\gamma^5 \left(K_p + K_s\right)^2\right]^{1/3} \tag{43}$$

$$V_{cr} = \left[\frac{3^7 \pi^4 \left(K_p + K_s\right)^2 \Delta\gamma^5}{\rho_p^3 d_p^5}\right]^{1/6} \tag{44}$$

A comparison of the impact velocity and the critical velocity as a function of particle diameter for steel particles approaching polystyrene filter led to the conclusion that thermal rebound occurs for sub-10 nm particles because of excessive impact velocity. The rebound is dependent on the mechanical constant and the specific adhesion energy. For particles greater than 10 nm, the impaction velocities are less than the critical velocity, so that the particles attach to the surface.

The effective single fiber efficiency (E_{eff}) based on consideration of the thermal rebound, is calculated as

$$E_{eff} = E \cdot \varepsilon \tag{45}$$

where E is the total single fiber efficiency and ε is the adhesion efficiency. In the conventional filtration theory, adhesion efficiency is considered to be a unity value; however, the value is actually less than one if thermal rebound occurs. The sticking efficiency due to the thermal rebound (ε) is defined as follows (Wang and Kasper, 1991):

$$\varepsilon = \int_0^{v_{cr}} f\left(v_{im}\right) dv_{im} \Big/ \int_0^{\infty} f\left(v_{im}\right) dv_{im} \tag{46}$$

With a Boltzmann distribution for the particle impact velocity the equation becomes

$$\varepsilon = \int_0^{1/TR} \left(\frac{32}{\pi^2}\right) x^2 \exp\left(-\frac{4x^2}{\pi}\right) dx \tag{47}$$

where TR is the thermal rebound coefficient that is the ratio of the mean impact velocity and the critical velocity. Calculating single fiber efficiency based on consideration of Brownian diffusion and interception and using the Lee and Liu (1982) equation, which does not consider gas slip for nanoparticles, results in misleading efficiency values greater than 1 for nanoparticles with diameters of approximately sub-10 nm.

Recently, Mouret *et al.* (2011) employed a Tabor parameter to demonstrate that the BH and JKR models used by Wang and Kasper are associated with the extremes of the Tabor spectrum. They concluded that for sub-100 nm particles, the Tabor value is less than 0.1, and the BH theory should be used for calculating the adhesion energy (Johnson, 1997; Mouret *et al.*, 2011). The researchers also

pointed out that the approximation of BH adhesion energy equation used by Wang and Kasper was inaccurate for sub-20 nm particles. Thus, they have employed Eq. (17) and showed that no thermal rebound occurs with steel nanoparticles down to 1 nm approaching copper filter, and they also demonstrated that the thermal rebound effect increases as the temperature rises; however, the temperature must be as high as 1000 K for thermal rebound to be observed (Mouret *et al.*, 2011). The modification theory of Mouret *et al.* (2011) is a reasonable conclusion in light of the reasons why most researchers are unable to verify thermal rebound.

As discussed earlier, adhesion energy models were employed in the calculation of particle critical velocity; however, the adhesion energy is dependent on material properties (Tsai *et al.*, 1991) such as Hamaker constant, mechanical constant of materials, surface adhesive energy per unit contact area and elastic yield stress. Some of these parameters are not available for nano-sized particles depending on the type of materials (Hartland, 2004); this affects the calculations of adhesion energy and nanoparticle critical velocity.

The Mouret *et al.* (2011) theory had the same problem that Wang and Kasper (1991) encountered in the calculation of single-fiber efficiency. They employed Lee and Liu (1982) and Stechkina and Fuchs (1968) equations that fail to consider gas slip and results the nanoparticle removal efficiency of greater than one. As a result, additional theoretical studies are needed for the determination of the critical particle diameter below which thermal rebound may occur.

Experimental Work

A large and growing body of literature includes respects related to whether or not thermal rebound leads to the reduction of filtration efficiency. Table 3 summarizes the experimental studies related to the thermal rebound theory and their results.

In all of the experimental work listed above, only three groups of researchers reported the thermal rebound of particles smaller than 2 nm, but they were likely misled because of instrument error. In 1984, researchers tested the filtering of silver nanoparticles as small as 3.5 nm through tube and screen-type diffusion batteries and showed that the nanoparticle penetration curves followed those of classical filtration theory (Scheibel and Porstendörfer, 1984). One criticism of this study is related to the material of the particles tested. Silver is a soft material that may not exhibit elastic behavior upon impact with a filter surface, so the plastic impaction that decreases the rebound velocity of the particle may lead to higher capturing efficiency. Another experimental study filtered silver particles as small as 4 nm and dioctylphthalate particles as small as 32 nm through fibrous and membrane filters, but the researchers observed no thermal rebound effect in their results (Van Osdell *et al.*, 1990). Multilayer filters may therefore not be an efficient device for determining the existence of thermal rebound, because rebounded particles from the upper layers may be captured by the other layers of the filter. Thus, although thermal rebound could be associated with nanoparticles, it appears to have no significant consequences in multilayer filters.

Otani *et al.* (1995) employed silver nanoparticles in the range of 1 nm to 10 nm, which were passed through wire screens and circular tubes. Their results show that nanoparticle penetration increases for nanoparticles with diameters less than 2 nm in circular tubes; however, thermal rebound did not affect particle penetration in wire screens (Otani *et al.*, 1995). The discrepancy between the particle penetration of wire screens and that in circular tubes appeared to be due to the capture of nanoparticles in the multilayers comprising wire screen filters. Also problematic is the fact that the results of the study relied too heavily on the accuracy of the DMA and FCE, which was in doubt at that time.

In another filtration efficiency study, eight stages of wire screens were used to filter out tested tungsten oxide and molybdenum oxide particles, and the thermal rebound effect was not observed (Skaptsov *et al.*, 1996). These particles are harder than NaCl particles and may exhibit elastic impaction; however, rebounded particles may also be captured by other stages.

Ichitsubo *et al.* (1996) carried out a study involving the penetration of NaCl and silver particles through a single-stage wire screen and showed the probability of thermal rebound for particles with sizes smaller than 2 nm. Their results also showed that the particle penetration trend is a function of the particle material for sub-2 nm particles, due to the differences in hardness of the materials: the greater the hardness, the higher the probability of particle rebound. One of the limitations of this study is that the size range of the particles may not be accurate because of the inaccuracy of the DMA and FCE available at that time. Alonso *et al.* (1997) employed a single-stage wire screen similar to the one used by Ichitsubo *et al.* (1996). Their experimental measurements obtained with the use of tandem DMA did not show particle rebound. They also concluded that using a single DMA for nanoparticle measurement had caused errors in previous studies so that earlier results were unreliable. In 2005, Heim *et al.* (2005) tested the filtration efficiency of charged and uncharged NaCl particles down to 2.5 nm in diameter through a metal and plastic filter and did not observe thermal rebound for small nanoparticles. Kim *et al.* (2006) later employed NaCl particles down to 1 nm to test the filtration efficiency of glass fibrous filters. A particle size magnifier was used prior to a condensation nucleus counter in order to increase the nanoparticle counting efficiency, especially for sub-10 nm particles. Their results showed that filtration efficiency decreases for charged and uncharged sub-2 nm particles due to the effect of thermal rebound. The method used to measure particle concentrations thus strongly affects conclusions with respect to thermal rebound for small nanoparticles. The question that needs to be answered is which equipment is associated with the greatest efficiency and is the most reliable for measuring nanoparticle concentrations.

In 2007 and 2008, a number of studies examined the validation of thermal rebound theory using a variety of particles (NaCl, DOP, and silver) and filters (fibrous filter, fiber glass, H&V, N95, P100, and stainless steel wire

Table 3. Experimental studies in thermal rebound theory.

References	Particle characteristics	Media type	Operating conditions and filter characteristics	Instrument	Results
Scheibel and Porstendörfer, 1984	Silver particles: 3.5 nm < dp < 130 nm	Tube and screen-type diffusion batteries	df = 0.005 cm α = 0.2798 U = 2.4 cm/s	EC DMA TEM	No thermal rebound
Van Osdell *et al.*, 1990	Silver particles: 4 nm < dp < 10 nm DOP particles: 32 nm < dp < 420 nm	Glass fiber filter, composite fiber filter, and membrane filter	df < 1 μm α = 0.069–0.078 U = 0.5–20 cm/s L = 0.035–0.470 mm	CNC EC	No thermal rebound
Otani *et al.*, 1995	Silver particles 1 nm < dp < 10 nm	Stainless steel wire screens, and circular aluminum tubes	Wire Screens: df = 52, 300 μm α = 0.293, 0.310 U = 1.2–3.6 cm/s ds = 4.2 cm Circular Tube: d = 6 mm L = 0.5, 1, 2 m	DMA FCE	Thermal rebound for dp < 2 nm in circular tubes
Skaptsov *et al.*, 1996	WO_3, and MoO_3 3.1 nm < dp < 15.4 nm	Stainless steel, and wire screen	Q = 2 lpm U = 2.92 cm/s T=295, 316, 337 K	EC UCPC	No thermal rebound
Ichitsubo *et al.*, 1996	Silver, and NaCl particles: 1 nm < dp < 7 nm	Single stage wire screen (Stainless steel type 316)	df =75 μm α = 0.289 Q = 6 lpm ds =32 mm	DMA FCE	Thermal rebound for dp < 2 nm
Alonso *et al.*, 1997	Silver, and NaCl particles: 1 nm < dp < 7 nm	Single stage wire screens, and tubes	df = 75 μm α = 0.289 Q = 1,3,6 lpm ds = 11, 32 mm	Tandem-DMA CNC	No thermal rebound
Heim *et al.*, 2005	NaCl (charged, uncharged) particles: 2.5 nm < dp < 20 nm	Stainless steel, nickel mesh, and polypropylene filter	df = 4.2 μm, α = 0.0022 df = 54.6 μm, α = 0.34 df = 110 μm, α = 0.387	DMA CPC	No thermal rebound
Kim *et al.*, 2006	NaCl (singly charged, uncharged, neutralized) particles: 1 nm < dp < 100 nm	Glass fibrous filters	df = 9.1, 11.8 μm Q = 4.4 lpm df = 4.15 cm U = 2.5 cm/s	Nano-DMA PSM-CNC	Thermal rebound for dp < 2 nm
Huang *et al.*, 2007	NaCl particles: 4.5 nm < dp < 10 μm	Fibrous filter for respiratory masks	df = 13 μm α = 0.035 Q = 30, 60, and 85 lpm	Long-DMA Nano-DMA CPC	No thermal rebound
Japuntich *et al.*, 2007	NaCl, dioctyl phthalate (DOP) particles: 10 nm < dp < 400 nm	Hollingsworth and Vose (H &V) Fiber glass filter	df = 1.9 to 4.9 μm α = 0.039 to 0.050	DMA SMPS	No thermal rebound
Kim *et al.*, 2007	Silver particles: 3 nm < dp < 20 nm	Hollingsworth and Vose (H &V) Fiber glass fibrous filter	df = 1.9 to 4.9 μm α = 0.039 to 0.050 U = 5.3,10, 0.15 m/s	UCPC DMA	No thermal rebound
Steffens and Coury, 2007	NaCl particles: 8.5 nm < dp < 94.8 nm	Polyester filter fiber filter of cellulose (HEPA)	α = 0.920 h = 0.4 mm df = 0.45 μm		No thermal rebound
Wang *et al.*, 2007	Silver particles: 3 nm < dp < 20 nm NaCl particles: 15 nm < dp < 400 nm	Hollingsworth and Vose (H &V) fiber glass filters: HE1073, HE1021, HF0031, HF0012	α = 0.05, 0.049, 0.047, and 0.039	Nano-DMA CPC	No thermal rebound
Rengasamy *et al.*, 2008	Silver particles: 4 nm < dp < 30 nm NaCl particles: 20 nm < dp < 400 nm	N95 and P100 filter	Q = 85 lpm	Nano DMA UCPC	No thermal rebound

Table 3. *(continued).*

References	Particle characteristics	Media type	Operating conditions and filter characteristics	Instrument	Results
Shin *et al.*, 2008	Silver particles: 3 nm < dp < 20 nm	Stainless steel wire screen	df = 90 μm T < 500 K	UCPC Nano DMA	No thermal rebound
Golanski *et al.*, 2009	Graphite particles: 10 nm < dp <100 nm	Fiber glass, HEPA, and electret	Basis weight 150, 85, and 75 g/m^2	SMPS	No thermal rebound
Van Gulijk *et al.*, 2009	NaCl, $CaCl_2$, $(NH_4)_2SO_2$, $NiSO_4$ electrically neutral 7 nm < dp < 20 nm	Stainless steel grid, and wire screen	df = 40 μm	EC CPC-SMPS	Possibility of thermal rebound for NaCl, $NiSO_4$
Heim *et al.*, 2010	Singly charged WO_x 1.2 nm < dp < 8 nm	Eclectically grounded metal wire grid	df = 54.4, 50.1, 101.2 μm α = 0.335, 0.313, 0.297	DMA FCE	No thermal rebound
Brochot *et al.*, 2011	Carbon, NaCl, copper particles: 5 nm < dp < 400 nm	Fiber glass	df =3.19 μm, 5.14 μm α = 0.05, 0.064 L = 552, 427 μm	Nano DMA UCPC CNC	No thermal rebound
Yamada *et al.*, 2011	NaCl particles: 10 nm < dp < 60 nm	Wire screen	df = 30, 60, 2.1, 9.5 μm α = 0.215, 0.276, 0.088, 0.172 L = 0.06, 0.12, 0.38, 0.28 mm	DMA CPC	No thermal rebound

screen), employing SMPS with long and nano DMA. No thermal rebound was observed for tests involving NaCl particles with diameters down to 4.5 nm, silver particles with diameters down to 3 nm, or DOP particles with diameters down to 10 nm. Particles below these sizes were not tested for (Huang *et al.*, 2007; Japuntich *et al.*, 2007; Kim *et al.*, 2007; Steffens and Coury, 2007; Wang *et al.*, 2007; Rengasamy *et al.*, 2008; Shin *et al.*, 2008).

In 2009, Golanski *et al.* (2009) filtered out graphite particles in the range of 10 nm to 100 nm through a fibrous and electret filter, with the filtration efficiency measured by SMPS showing no thermal rebound effect. In the same year, Van Gulijk *et al.* (2009) measured the nanoparticle removal efficiency of a variety of electrically neutral particles (NaCl, $CaCl_2$, $(NH_4)_2SO_2$, and $NiSO_4$) with diameters ranging from 7 nm to 20 nm passed through a stainless steel screen. Their results indicated the possibility of thermal rebound occurrence for NaCl and $NiSO_4$ nanoparticles. Based on which they postulated that the lower sticking efficiency was due to salt particles having a lower Hamaker constant than metal particles, which increases the effect of thermal rebound. Neutral nanoparticles have a lower sticking probability than charged particles due to the weaker image forces between the nanoparticles and a surface (Van Gulijk *et al.*, 2009).

In another study by Heim *et al.* (2010) DMA and FCE were used to measure the penetration of singly charged tungsten nanoparticles ranges from 1.2 nm to 8 nm through three different wire grids. In that study, no thermal rebound was observed for tungsten particles, and the lower penetration measured for sub-3 nm particles was attributed to the smaller image forces. In the same year Brochot *et al.* (2011) employed a variety of nanoparticles (carbon, NaCl, and copper) ranging from 5 nm to 400 nm passed through fiber glass filters. The particle concentration measurements using nano DMA, CNC, and UCPC did not reveal thermal rebound effect. However, the discrepancies among the penetration levels of NaCl, carbon, and copper nanoparticles indicated that the morphology of the nanoparticles affects the efficiency of particle removal (Brochot *et al.*, 2011).

Yamada *et al.* (2010) passed NaCl particles in the size range of 10 nm to 60 nm through different wire screens in order to determine the effect of a non-uniformly packed filter on particle-removal efficiency. Their results showed that the efficiency measured aligned with classical filtration theory with no thermal rebound being observed (Yamada *et al.*, 2011).

Most thermal rebound researchers considered the STP conditions and did not take into account the effect of gas pressure on the thermal rebound theory. Recently, Rennecke and Weber (2013a) conducted a numerical analysis and experiments in order to understand whether thermal rebound is pressure dependent for nanoparticles; they found that the collection efficiency of a low-pressure impactor and impact velocity decreased with the increase of the chamber pressure. Furthermore, in another study (Rennecke and Weber, 2013b) they showed that dense NaCl nanoparticles had a higher chance to rebound in the low pressure impactor than porous NaCl and dense spherical silver nanoparticles did. This result is in contradiction to other experimental studies, which did not show the possibility of thermal rebound for NaCl nanoparticles. The disagreement is likely because the drag force at ambient pressure leads to the nanoparticle energy loss prior to nanoparticle rebound; consequently, a nanoparticle is likely to be captured by a surface.

In summary, researchers have employed a variety of methodologies for experimental measurement as a means of minimizing uncertainties based on the sampling method, filter holder design, electrostatic effect, morphology effect, particle type, and measurement method. Most of the experimental studies led to the conclusion that particle

removal efficiency increases with decreased particle size, and no thermal rebound was observed. The key finding of these studies is that thermal rebound may not present a significant problem with multilayer filters because rebounded particles may be captured by the other layers. Only a few of the studies dealt with single-fiber efficiency; however, in those studies, the reliability of the measurement equipment was inadequate. Improved studies are needed with respect to examining the filtration efficiency of monodisperse nanoparticles through a single-stage wire screen with more reliable equipment. The filtration efficiencies of a single-stage wire screen in a uniform structure are more similar to the theoretical simulations due to the elimination of the effect of inhomogeneity of the filter on nanoparticle filtration efficiency. Employing monodisperse nanoparticles instead of polydisperse ones could minimize the nanoparticle concentration measurement errors as well. In conclusion, no convincing results have been produced that either prove or disprove the thermal rebound theory. A need exists for an investigation of the effects of thermal rebound and a determination of whether those effects prevent the capture of nanoparticles by conventional filters.

KNOWLEDGE GAP AND RESEARCH NEEDED

Although there have been many advances in nanoparticle filtration; there is still need to consider the effect of thermal rebound on filters. A number of assumptions underlie in the theoretical and experimental studies. It was assumed that the impact velocity of particles follows a Maxwell-Boltzmann distribution; while this distribution is for ideal gas molecules, the validity of its use for nanoparticles is in doubt. In previous studies, JKR and BH models have been employed to calculate the adhesion energy between bodies. Both models assume elastic impaction between the bodies, but fail to consider the implications if nanoparticle impaction is completely plastic and energy loss is not neglected. Thus, the particle-surface adhesion energy based on plastic deformation should be considered for calculating the nanoparticle critical velocity.

JKR and BH models which are employed in previous studies are validated for micron particles; however, the impact mechanisms for microscale and nanoscale particles deviate because latter must include consideration of molecular interactions (Teodorescu and Rahnejat, 2007). Thus, the selection of a contact model that accounts for both scales is always based on underlying assumptions. These models require the exact value of the mechanical constant, Hamaker constant, and the specific adhesion energy between bodies; however, such exact values are unavailable for most materials. Also, a further question arises here if these parameters are size-independent and they are the same for bulk materials and nanoparticles. Studies show that the material properties of nanoscale bodies differ from those of bulk materials. Nanomaterials also have higher yield stresses than bulk materials (Richter *et al.*, 2009). Thus, incorporating the material properties of nanoparticles based on those bulk materials may lead to inaccuracies in the thermal rebound theory. Another study revealed that the nonlocal dielectric properties of materials affect the Hamaker constant for small nanoparticles (Esquivel-Sirvent and Schatz, 2012), and Pinchuk later indicated that the Hamaker constant is greater for nanoparticles smaller than the mean free path of electrons with diameters in the order of 2 nm (Pinchuk, 2012). Thus, the size dependence of the dielectric properties of nanoparticles means that the Hamaker constant is also size dependent for the nanoparticles that will be considered in future studies. Furthermore, previous studies relied on a variety of ranges of specific adhesion energy requirements in contact adhesion models. Wang and Kasper (1991) based their work on $\Delta\gamma = 0.01 J/m^2$; however, Mouret *et al.* (2011) later pointed out that the specific adhesion energy in the Wang and Kasper's research should be $\Delta\gamma = 0.005 J/m^2$. Rennecke *et al.* (2013) used a value of 0.5 for NaCl particles (Mulheran, 1994; Rennecke and Weber, 2013c). A great deal of uncertainty is thus related to the determination of the amount of specific adhesion energy especially in the case of nanomaterials.

Theories of particle-surface adhesion energy apply to smooth surfaces; however, the surfaces of the nanoparticles and the filter are not smooth, so including consideration of surface roughness is essential. Rebound velocity has been reported to depend on material properties and surface topography (Chang and Ling, 1991). Surface roughness can play an important role in the determination of the adhesion force between nanoparticles and a wavy surface (Delrio *et al.*, 2005). It has been found that surface roughness affects the surface force, the interaction in terms of specific adhesion energy, the impact mechanisms, the energy exchange, and particle rebound (Tabor, 1977; Broom, 1979; Paw U, 1983; Tsai *et al.*, 1990). Consideration of contact adhesion models for wavy surfaces should thus be included in the thermal rebound theory.

Although impaction velocity has 6 directions (+x, –x, +y, –y, +z, –z), only impaction along normal direction is considered in existing thermal rebound models and analysis. Particles may collide with the surface obliquely and the tangential component of the impact velocity may contribute to the probability of either adhesion or rebound. The effect of the impaction angle on thermal rebound theory is still uncertain. Oblique impaction could affect the coefficient of restitution and the critical velocity and, consequently, influence the probability of the occurrence of thermal rebound, a factor that has not been considered in previous thermal rebound theories. A normal impact velocity contributes to deformation, and a tangential velocity promotes particle rotation and enlarges the contact area. A tangential force causes shear stress which creates a horizontal shift from the contact area (Savkoor and Briggs, 1977). As a result, including consideration of oblique particle impaction may change the thermal rebound theory because this factor was neglected in previous studies. It has been pointed out that the critical velocity for a particle to be captured in oblique impaction is lower than that negotiated for perpendicular impaction (Broom, 1979; Aylor and Ferrandino, 1985). Studies have shown that the rebound velocity for smaller impact angles is higher than that for larger angles and that the coefficient of restitution decreases with increases in

incident angle of the impact (Tabakoff and Malak, 1987). Including consideration of oblique impaction in elastic and plastic impaction is therefore important. A number of studies have demonstrated the importance of the tangential forces with respect to the rebound angle in elastic impactions (Maw *et al.*, 1976; Maw *et al.*, 1981). It has also been reported that that plastic deformation can dispel the initial kinetic energy in oblique impactions and can affect rebound behavior, especially at high impaction angles (Wu *et al.*, 2008).

In reality, drag force may also affect the rolling and detachment of particles on the filter surface (Liu *et al.*, 2011). However this important factor is omitted in existing thermal rebound theory. This also helps explain the discrepancy between the thermal rebound models and experimental work. Addressing all the current knowledge gaps may eliminate the needs for considering the thermal rebound in a certain way.

CONCLUSIONS

This review paper has discussed nanoparticle filtration and the thermal rebound theory of nanoparticles. While methods have been developed for calculating the single-fiber efficiency of micron particles, doubt still exists with respect to the calculation of the single-fiber efficiency of nanoparticles. The theoretical analysis of single-fiber efficiency with respect to nanoparticles is approximate because it has been based on validations for micron particles. A better understanding of the physical properties specific to nanoparticles could lead to the design of high-performance filters for collecting nanoparticles.

In spite of the investigation of the thermal rebound theory for airborne nanoparticles in numerous studies, since its development, no convincing results have clearly demonstrated the role of thermal rebound, if any, in nanoparticle filtration. Neither the JKR nor the BH adhesion energy model is suitable for calculating the adhesion energy between nanoparticles and a surface. More accurate theoretical analysis and experiments are thus required in order to prove or disprove the thermal rebound theory.

ACKNOWLEDGMENT

The authors acknowledge the financial support from Natural Science and Engineering research Council (NSERC).

REFERENCES

Allen, T.M. and Cullis, P.R. (2004). Drug Delivery Systems: Entering the Mainstream. *Science* 303: 1818–1822.

Alonso, M., Kousaka, Y., Hashimoto, T. and Hashimoto, N. (1997). Penetration of Nanometer-sized Aerosol Particles through Wire Screen and Laminar Flow Tube. *Aerosol Sci. Technol.* 27: 471–480.

Ayesh, A.I., Brown, S.A., Awasthi, A., Hendy, S.C., Convers, P.Y. and Nichol, K. (2010). Coefficient of Restitution for Bouncing Nanoparticles. *Phys. Rev. B: Condens. Matter*. 81: 195422 (5 Pages).

Aylor, D.E. and Ferrandino, F.J. (1985). Rebound of Pollen and Spores during Deposition on Cylinders by Inertial Impaction. *Atmos. Environ.* 19: 803–806.

Bałazy, A., Podgórski, A. and Gradoń, L. (2004). Filtration of Nanosized Aerosol Particles in Fibrous Filters. I - Experimental Results. *J. Aerosol Sci.* 35: S967–S968.

Bałazy, A. and Podgórski, A. (2007). Deposition Efficiency of Fractal-like Aggregates in Fibrous Filters Calculated Using Brownian Dynamics Method. *J. Colloid Interface Sci.* 311: 323–337.

Barhate, R.S. and Ramakrishna, S. (2007). Nanofibrous Filtering Media: Filtration Problems and Solutions from Tiny Materials. *J. Membr. Sci.* 296: 1–8.

Boskovic, L., Altman, I.S., Agranovski, I.E., Braddock, R.D., Myojo, T. and Choi, M. (2005). Influence of Particle Shape on Filtration Processes. *Aerosol Sci. Technol.* 39: 1184–1190.

Boskovic, L., Agranovski, I.E., Altman, I.S. and Braddock, R.D. (2008). Filter Efficiency as a Function of Nanoparticle Velocity and Shape. *J. Aerosol Sci.* 39: 635–644.

Bradley, R. (1932). The Cohesive Force between Solid Surfaces and the Surface Energy of Solids, London, Edinburgh, and Dublin Philosophical Magazine and Journal of Science, Taylor & Francis, 13: 853–862.

Brochot, C., Mouret, G., Michielsen, N., Chazelet, S. and Thomas, D. (2011). Penetration of Nanoparticles in 5 nm to 400 nm size Range through two Selected Fibrous Media. *J. Phys: Conf. Ser.* 304: 012068, doi: 10.1088/1742-6596/304/1/012068.

Broom, G.P. (1979). Adhesion of Particles in Fibrous Filters. *Filtr. Sep.* 16: 661–662, 664.

Brown, R.C. (1993). *Air Filtration: An Integrated Approach to the Theory and Applications of Fibrous Filters*, Pergamon Press, Oxford.

Buseck, P.R. and Adachi, K. (2008). Nanoparticles in the Atmosphere. *Elements* 4: 389–394.

Castellano, P., Ferrante, R., Curini, R. and Canepari, S. (2009). An Overview of the Characterization of Occupational Exposure to Nanoaerosols in Workplaces. *J. Phys: Conf. Ser.* 170: 012009, doi: 10.1088/1742-6596/170/1/012009.

Chang, W. and Ling, F.F. (1991). Normal Impact Model of Rough Surfaces. *J. Tribol.* 114: 439–447.

Chen, C. and Huang, S. (1998). The Effects of Particle Charge on the Performance of a Filtering Facepiece. *Am. Ind. Hyg. Assoc. J.* 59: 227–233.

Choi, J., Park, S. and Kim, S. (2007). A Brownian Dynamics Simulation Method for Analyzing Particle Behavior in Nonuniform and Alternating Electric Fields. *J. Aerosol Sci.* 38: 192–210.

Dahneke, B. (1971). The Capture of Aerosol Particles by Surfaces. *J. Colloid Interface Sci.* 37: 342–353.

Delrio, F.W., De Boer, M.P., Knapp, J.A., Reedy, Jr. E.D., Clews, P.J. and Dunn, ML. (2005). The Role of van der Waals Forces in Adhesion of Micromachined Surfaces. *Nat. Mater.* 4: 629–634.

Derjaguin, B., Muller, V. and Toporov, Y.P. (1975). Effect of Contact Deformations on the Adhesion of Particles. *J. Colloid Interface Sci.* 53: 314–326.

Donaldson, K., Tran, L., Jimenez, L.A., Duffin, R., Newby,

D.E., Mills, N., MacNee, W. and Stone, V. (2005). Combustion-derived Nanoparticles: A Review of Their Toxicology Following Inhalation Exposure. *Part. Fibre Toxicol.* 2: 10.

Elsaesser, A. and Howard, C.V. (2012). Toxicology of Nanoparticles. *Adv. Drug Delivery Rev.* 64: 129–137.

Esquivel-Sirvent, R. and Schatz, G.C. (2012). Spatial Nonlocality in the Calculation of Hamaker Coefficients. *J. Phys. Chem. C*. 116: 420–424.

Golanski, L., Guiot, A., Rouillon, F., Pocachard, J. and Tardif, F. (2009). Experimental Evaluation of Personal Protection Devices against Graphite Nanoaerosols: Fibrous Filter Media, Masks, Protective Clothing, and Gloves. *Hum. Exp. Toxicol.* 28: 353–359.

Golanski, L., Guiot, A. and Tardif, F. (2010). Experimental Evaluation of Individual Protection Devices against Different Types of Nanoaerosols: Graphite, TiO_2, and Pt. *J. Nanopart. Res.* 12: 83–89.

Gómez, V., Huang, C.H., Alguacil, F.J. and Alonso, M. (2012). Deposition of Aerosol Particles below 10 nm on a Mixed Screen-type Diffusion Battery. *Aerosol Air Qual. Res.* 12: 295–299

Greenwood, J.A. (1997). Adhesion of Elastic Spheres. *Proc. R. Soc. London, Ser. A* 453: 1277–1297.

Hartland, G.V. (2004) Measurements of the Material Properties of Metal Nanoparticles by Time-resolved Spectroscopy. *Phys. Chem. Chem. Phys*. 6: 5263–5274.

Heim, M., Mullins, B.J., Wild, M., Meyer, J. and Kasper, G. (2005). Filtration Efficiency of Aerosol Particles below 20 Nanometers. *Aerosol Sci. Technol*. 39: 782–789.

Heim, M., Attoui, M. and Kasper, G. (2010). The Efficiency of Diffusional Particle Collection onto Wire Grids in the Mobility Equivalent Size Range of 1.2-8 nm. *J. Aerosol Sci.* 41: 207–222.

Hinds, W.C. (1999). *Aerosol Technology Properties, Behevior, and Measurment of Airborne Particles*, Wiley - Interscience.

Hofmann, W., Morawska, L., Winkler-Heil, R. and Moustafa, M. (2009). Deposition of Combustion Aerosols in the Human Respiratory Tract: Comparison of Theoretical Predictions with Experimental Data Considering Nonspherical Shape. *Inhalation Toxicol.* 21: 1154–1164.

Huang, S., Chen, C., Chang, C., Lai, C. and Chen, C. (2007). Penetration of 4.5 nm to 10 μm Aerosol Particles through Fibrous Filters. *J. Aerosol Sci.* 38: 719–727.

Hung, C. and Leung, W.W. (2011). Filtration of Nano-aerosol Using Nanofiber Filter under Low Peclet Number and Transitional Flow Regime. *Sep. Purif. Technol.* 79: 34–42.

Hunter, S.C. (1957). Energy Absorbed by Elastic Waves during Impact. *J. Mech. Phys. Solids* 5: 162–171.

Hutchings, I. (2001). Energy Absorbed by Elastic Waves during Plastic Impact. *J. Phys. D: Appl. Phys.* 12: 1819.

Ichitsubo, H., Hashimoto, T., Alonso, M. and Kousaka, Y. (1996). Penetration of Ultrafine Particles and Ion Clusters through Wire Screens. *Aerosol Sci. Technol*. 24: 119–127.

Intra, P. and Tippayawong, N. (2011). An Overview of Unipolar Charger Developments for Nanoparticle Charging. *Aerosol Air Qual. Res.* 11: 187–209.

Japuntich, D.A., Franklin, L.M., Pui, D.Y., Kuehn, T.H., Kim, S.C. and Viner, A.S. (2007). A Comparison of Two Nano-sized Particle Air Filtration Tests in the diameter Range of 10 to 400 Nanometers. *J. Nanopart. Res.* 9: 93–107.

Jawahar, N. and Reddy, G. (2012). Nanoparticles: A Novel Pulmonary Drug Delivery System for Tuberculosis. *J. Pharm. Sci. Res*. 4: 1901–1906.

Johnson, K., Kendall, K. and Roberts, A. (1971). Surface Energy and the Contact of Elastic Solids. *Proc. R. Soc. London, Ser. A* 324: 301–313.

Johnson, K.L. (1997). Adhesion and Friction between a Smooth Elastic Spherical Asperity and a Plane Surface. *Proc. R. Soc. London, Ser. A* 453: 163–179.

Johnson, K.L. and Greenwood, J.A. (1997). An Adhesion Map for the Contact of Elastic Spheres. *J. Colloid Interface Sci.* 192: 326–333.

Jung, J.H., Oh, H.C., Noh, H.S., Ji, J.H. and Kim, S.S. (2006). Metal Nanoparticle Generation Using a Small Ceramic Heater with a Local Heating Area. *J. Aerosol Sci.* 37: 1662–1670.

Jung, S., Suh, D. and Yoon, W. (2010). Molecular Dynamics Simulation on the Energy exchanges and Adhesion Probability of a Nano-sized Particle Colliding with a Weakly Attractive Static Surface. *J. Aerosol Sci.* 41: 745–759.

Kim, C.S., Bao, L., Okuyama, K., Shimada, M. and Niinuma, H. (2006). Filtration Efficiency of a Fibrous Filter for Nanoparticles. *J. Nanopart. Res.* 8: 215–221.

Kim, S.C., Harrington, M.S. and Pui, D.Y.H. (2007). Experimental Study of Nanoparticles Penetration through Commercial Filter Media. *J. Nanopart. Res.* 9: 117–125.

Kirsch, A.A. and Fuchs, N.A. (1968). Studies on Fibrous Aerosol Filters-III Diffusional Deposition of Aerosols in Fibrous Filters. *Ann. Occup. Hyg.* 11: 299–304.

Kittelson, D.B. (1998). Engines and Nanoparticles: A Review. *J. Aerosol Sci.* 29: 575–588.

Kreyling, W.G., Semmler-Behnke, M. and Möller, W. (2006). Health Implications of Nanoparticles. *J. Nanopart. Res.* 8: 543–562.

Krish, A.A. and Stechkina, I.B. (1978). The Theory of Aerosol Filtration with Fibrous Filters, In *Fundamentals of Aerosol Science*, Shaw, D.T., (Ed.), Wiley, New York.

Krupp, H. (1967) Particle Adhesion Theory and Experiment. *Adv. Colloid Interface Sci.* 1: 111–239

Kuwabara, S. (1959). The Forces Experienced by Randomly Distributed Parallel Circular Cylinders or Spheres in a Viscous Flow at Small Reynolds Numbers. *J. Phys. Soc. Jpn.* 14: 527.

Lee, K.W. and Gieseke, J.A. (1980). Note on the Approximation of Interceptional Collection Efficiencies. *J. Aerosol Sci.* 11: 335–341.

Lee, K.W. and Liu, B.Y.H. (1982). Theoretical Study of Aerosol Filtration by Fibrous Filters. *Aerosol Sci. Technol.* 1: 147–161.

Leob, L.B. (1961). *The Kinetic Theory of Gases*, Dover, New York.

Lim, J., Yu, L.E., Kostetski, Y.Y., Lim, C., Ryu, J. and

Kim, J. (2008). Effects of Driving Conditions on Diesel Exhaust Particulates. *J. Air Waste Manage. Assoc.* 58: 1077–1085.

Lim, J., Lim, C. and Liya, E.Y. (2009). Composition and Size Distribution of Metals in Diesel Exhaust Particulates. *J. Environ. Monit.* 11: 1614–1621.

Lin, L., Lin, C., Lin, Y. and Chuang, K. (2009). The Effects of Indoor Particles on Blood Pressure and Heart Rate among Young Adults in Taipei, Taiwan. *Indoor Air* 19: 482–488.

Liu, B. and Rubow, K. (1990). Efficiency, Pressure Drop and Figure of Merit of High Efficiency Fibrous and Membrane Filter Media, 5th World Filtration Congress, Nice, France.

Liu, C.N., Chien, C.L., Lo, C.C., Lin, G.Y., Chen, S.C. and Tsai, C.J. (2011). Drag Coefficient of a Spherical Particle Attached on the Flat Surface. *Aerosol Air Qual. Res.* 11: 482–486.

Mandl, F. (1988). *Statistical Physics*, Chichester, West Sussex, The Manchester Physics Series, Wiley, New York.

Marra, J., Voetz, M. and Kiesling, H. (2010). Monitor for Detecting and Assessing Exposure to Airborne Nanoparticles. *J. Nanopart. Res.* 12: 21–37.

Maugis, D. and Pollock, H.M. (1984). Surface Forces, Deformation and Adherence at Metal Microcontacts. *Acta Metall.* 32: 1323–1334.

Maugis, D.D. (2000). *Contact, Adhesion and Rupture of Elastic Solids*, Springer, Berlin, New York.

Maw, N., Barber, J.R. and Fawcett, J.N. (1976). The Oblique Impact of Elastic Spheres. *Wear* 38: 101–114.

Maw, N., Barber, J.R. and Fawcett, J.N. (1981). Role of Elastic Tangential Compliance in Oblique Impact. *J. Lubr. Technol.* 103: 74–80.

McKenna, J.D., Turner, J.H. and McKenna, J.P. (2008). *Fine Particle (2.5 Microns) Emissions: Regulation, Measurement, and Control*, Hoboken, Wiley, N.J.

Mengersen, K., Morawska, L., Wang, H., Murphy, N., Tayphasavanh, F., Darasavong, K. and Holmes, N.S. (2011). Association between Indoor Air Pollution Measurements and Respiratory Health in Women and Children in Lao PDR. *Indoor Air* 21: 25–35.

Miguel, A.F. (2003). Effect of Air Humidity on the Evolution of Permeability and Performance of a Fibrous Filter during Loading with Hygroscopic and Non-hygroscopic Particles. *J. Aerosol Sci.* 34: 783–799.

Motzkus, C., Chivas-Joly, C., Guillaume, E., Ducourtieux, S., Saragoza, L., Lesenechal, D., MacÉ, T., Lopez-Cuesta, J. and Longuet, C. (2012). Aerosols Emitted by the Combustion of Polymers Containing Nanoparticles. *J. Nanopart. Res.* 14.

Mouret, G., Chazelet, S., Thomas, D. and Bemer, D. (2011). Discussion about the Thermal Rebound of Nanoparticles. *Sep. Purif. Technol.* 78: 125–131.

Mulheran, P.A. (1994). Surface Free-energy Calculations and the Equilibrium Shape of NaCl Crystals. *Modell. Simul. Mater. Sci. Eng.* 2: 1123–1129.

Muller, V., Yushchenko, V. and Derjaguin, B.V. (1980). On the Influence of Molecular Forces on the Deformation of an Elastic Sphere and Its Sticking to a Rigid Plane. *J. Colloid Interface Sci.* 77: 91–101.

Nazarboland, M., Chen, X., Hearle, J., Lydon, R. and Moss, M. (2007). Effect of Different Particle Shapes on the Modelling of Woven Fabric Filtration. *J. Inf. Comput. Sci*. 2: 111–118.

Oberdörster, G., Gelein, R.M., Ferin, J. and Weiss, B. (1995). Association of Particulate Air Pollution and Acute Mortality: Involvement of Ultrafine particles? *Inhalation Toxicol.* 7: 111–124.

Oberdörster, G., Oberdörster, E. and Oberdörster, J. (2005). Nanotoxicology: An Emerging Discipline Evolving from Studies of Ultrafine Particles. *Environ. Health Perspect*. 113: 823–839.

Oberdörster, G., Stone, V. and Donaldson, K. (2007). Toxicology of Nanoparticles: A Historical Perspective. *Nanotoxicology* 1: 2–25.

Otani, Y., Emi, H., Cho, S.J. and Namiki, N. (1995). Generation of Nanometer Size Particles and Their Removal from Air. *Adv. Powder Technol.* 6: 271–281.

Paur, H., Cassee, F.R., Teeguarden, J., Fissan, H., Diabate, S., Aufderheide, M., Kreyling, W.G., Hänninen, O., Kasper, G., Riediker, M., Rothen-Rutishauser, B. and Schmid, O. (2011). In-vitro Cell Exposure Studies for the Assessment of Nanoparticle Toxicity in the Lung-A Dialog between Aerosol Science and Biology. *J. Aerosol Sci.* 42: 668–692.

Paw U, K.T. (1983). The Rebound of Particles from Natural Surfaces. *J. Colloid Interface Sci.* 93: 442–452.

Payet, S., Boulaud, D., Madelaine, G. and Renoux, A. (1992). Penetration and Pressure Drop of a HEPA Filter during Loading with Submicron Liquid Particles. *J. Aerosol Sci.* 23: 723–735.

Pich, J. (1965). The Filtration Theory of Highly Dispersed Aerosols. *Staub Reinhalt.* 5: 16–23.

Pich, J. (1966). The Effectiveness of the Barrier Effect in Fiber Filters at Small Knudsen Numbers. *Staub Reinhalt*. 26: 1–4.

Pinchuk, A.O. (2012). Size-dependent Hamaker Constant for Silver Nanoparticles. *J. Phys. Chem. C.* 116: 20099–20120.

Podgórski, A., Bałazy, A. and Gradoń, L. (2006). Application of Nanofibers to Improve the Filtration Efficiency of the Most Penetrating Aerosol Particles in Fibrous Filters. *Chem. Eng. Sci.* 61: 6804–6815.

Podgórski, A. and Bałazy, A. (2008). Novel Formulae for Deposition Efficiency of Electrically Neutral, Submicron Aerosol Particles in Bipolarly Charged Fibrous Filters Derived Using Brownian Dynamics Approach. *Aerosol Sci. Technol*. 42: 123–133.

Przekop, R. and Gradoń, L. (2008). Deposition and Filtration of Nanoparticles in the Composites of Nano- and Microsized Fibers. *Aerosol Sci. Technol.* 42: 483–493.

Qin, X. and Wang, S. (2006). Filtration Properties of Electrospinning Nanofibers. *J. Appl. Polym. Sci.* 102: 1285–1290.

Rahmat, M., Ghiasi, H. and Hubert, P. (2012). An Interaction Stress Analysis of Nanoscale Elastic Asperity Contacts. *Nanoscale* 4: 157–166.

Rengasamy, S., King, W.P., Eimer, B.C. and Shaffer, R.E. (2008). Filtration Performance of NIOSH-approved N95 and P100 Filtering Facepiece Respirators against 4 to 30

Nanometer-size Nanoparticles. *J. Occup. Environ. Hyg.* 5: 556–564.

Rennecke, S. and Weber, A.P. (2013a). A Novel Model for the Determination of Nanoparticle Impact Velocity in Low Pressure Impactors. *J. Aerosol Sci.* 55: 89–103.

Rennecke, S. and Weber, A.P. (2013b). On the pressure Dependence of Thermal Rebound. *J. Aerosol Sci.* 58: 129–134.

Rennecke, S. and Weber, A.P. (2013c). The Critical Velocity for Nanoparticle Rebound Measured in a Low Pressure Impactor. *J. Aerosol Sci.* 58: 135–147.

Richter, G., Hillerich, K., Gianola, D.S., Mönig, R., Kraft, O. and Volkert, C.A. (2009). Ultrahigh Strength Single Crystalline Nanowhiskers Grown by Physical Vapor Deposition. *Nano Lett*. 9: 3048–3052.

Roduner, E. (2006). Size Matters: Why Nanomaterials are Different. *Chem. Soc. Rev.* 35: 583–592.

Sato, S., Chen, D.R. and Pui, D.Y.H. (2007). Molecular Dynamics Study of Nanoparticle Collision with a Surface–Implication to Nanoparticle Filtration. *Aerosol Air Qual. Res.* 7: 278–303.

Savkoor, A.R. and Briggs, G.A.D. (1977). The Effect of Tangential Force on the Contact of Elastic Solids in Adhesion. *Proc. R. Soc. London, Ser. A* 356: 103–114.

Scheibel, H.G. and Porstendörfer, J. (1984). Penetration Measurements for Tube and Screen-type Diffusion Batteries in the Ultrafine Particle Size Range. *J. Aerosol Sci.* 15: 673–682.

Shin, W.G., Mulholland, G.W., Kim, S.C. and Pui, D.Y.H. (2008). Experimental Study of Filtration Efficiency of Nanoparticles below 20 nm at Elevated Temperatures. *J. Aerosol Sci.* 39: 488–499.

Skaptsov, A.S., Baklanov, A.M., Dubtsov, S.N., Laulainen, N.S., Sem, G. and Kaufman, S. (1996). An Experimental Study of the Thermal Rebound Effect of Nanometer Aerosol Particles. *J. Aerosol Sci.* 27: S145–S146.

Stechkina, I.B. (1966). Diffusion Precipitation of Aerosols in Fiber Filters. *Dokl. Akad. Nauk. SSSR* 167: 1327–1330.

Steffens, J. and Coury, J.R. (2007a). Collection Efficiency of Fiber Filters Operating on the Removal of Nano-sized Aerosol Particles: I-Homogeneous Fibers. *Sep. Purif. Technol.* 58: 99–105.

Steffens, J. and Coury, J.R. (2007b). Collection Efficiency of fiber Filters Operating on the Removal of Nano-sized Aerosol Particles. II. Heterogeneous Fibers. *Sep. Purif. Technol.* 58: 106–112.

Stevens, A.B. and Hrenya, C.M. (2005). Comparison of Soft-sphere Models to Measurements of Collision Properties during Normal Impacts. *Powder Technol.* 154: 99–109.

Sztuk, E., Przekop, R. and Gradoń, L. (2012). Brownian Dynamics for Calculation of the Single Fiber Deposition Efficiency of Submicron Particles. *Chem. Process Eng.* 33: 279–290.

Tabakoff, W. and Malak, M.F. (1987). Laser Measurements of Fly Ash Rebound Parameters for Use in Trajectory Calculations. *J. Turbomach.* 109: 535–540.

Tabor, D. (1948). A Simple Theory of Static and Dynamic Hardness. *Proc. R. Soc. London, Ser. A* 192: 247–274.

Tabor, D. (1977). Surface Forces and Surface Interactions. *J. Colloid Interface Sci.* 58: 2–13.

Teodorescu, M. and Rahnejat, H. (2007). Dry and Wet Nano-scale Impact Dynamics of Rough Surfaces with or without a Self-assembled Monolayer, Proceedings of the Institution of Mechanical Engineers, Part N: Journal of Nanoengineering and Nanosystems, 221: 49–58.

Tiwari, G., Tiwari, R., Sriwastawa, B., Bhati, L., Pandey, S., Pandey, P. and Bannerjee, S.K. (2012). Drug Delivery Systems: An Updated Review. *Int. J. Pharm. Invest.* 2: 2–11.

Torkmahalleh, M.A., Goldasteh, I., Zhao, Y., Udochu, N.M., Rossner, A., Hopke, P.K. and Ferro, A.R. (2012). $PM_{2.5}$ and Ultrafine Particles Emitted during Heating of Commercial Cooking Oils. *Indoor Air* 22: 483–491.

Tsai, C.J, Pui, D.Y.H. and Liu, B.Y.H. (1990). Capture and Rebound of Small Particles upon Impact with Solid Surfaces. *Aerosol Sci. Technol*. 12: 497–507.

Tsai, C.J, Pui, D.Y.H. and Liu, B.Y.H. (1991). Elastic Flattening and Particle Adhesion. *Aerosol Sci. Technol.* 15: 239–255.

Tsai, C.S., White, D., Rodriguez, H., Munoz, C.E., Huang, C., Tsai, C., Barry, C. and Ellenbecker, M.J. (2012). Exposure Assessment and Engineering Control Strategies for Airborne Nanoparticles: An Application to Emissions from Nanocomposite Compounding Processes. *J. Nanopart. Res*. 14: 989.

Tsai, S., Ashter, A., Ada, E., Mead, J.L., Barry, C.F. and Ellenbecker, M.J. (2008). Airborne Nanoparticle Release Associated with the Compounding of Nanocomposites Using Nanoalumina as Fillers. *Aerosol Air Qual. Res.* 8: 160–177.

Van Dijk, W.D., Gopal, S. and Scheepers, P.T.J. (2011). Nanoparticles in Cigarette Smoke; Real-time Undiluted Measurements by a Scanning Mobility Particle Sizer. *Anal. Bioanal.Chem.* 399: 3573–3578.

Van Gulijk, C., Bal, E. and Schmidt-Ott, A. (2009). Experimental Evidence of Reduced Sticking of Nanoparticles on a Metal Grid. *J. Aerosol Sci.* 40: 362–369.

Van Osdell, D.W., Liu, B.Y.H., Rubow, K.L. and Pui, D.Y.H. (1990). Experimental Study of Sub-micrometer and Ultrafine Particle Penetration and Pressure Drop for High Efficiency Filters. *Aerosol Sci. Technol*. 12: 911–925.

Wall, S., John, W. and Wang, H. (1990). Measurements of Kinetic Energy Loss for Particles Impacting Surfaces. *Aerosol Sci. Technol*. 12: 926–946.

Wallace, L.A., Emmerich, S.J. and Howard-Reed, C. (2004). Source Strengths of Ultrafine and Fine Particles Due to Cooking with a Gas Stove. *Environ. Sci. Technol.* 38: 2304–2311.

Wang, C. and Otani, Y. (2013). Removal of Nanoparticles from Gas Streams by Fibrous Filters: A Review. *Ind. Eng. Chem. Res*. 52: 5–17.

Wang, H. and Kasper, G. (1991). Filtration efficiency of nanometer-size aerosol particles. *J. Aerosol Sci.* 22: 31–41.

Wang, J., Chen, D.R. and Pui, D.Y.H. (2007). Modeling of Filtration Efficiency of Nanoparticles in Standard Filter

Media. *J. Nanopart. Res*. 9: 109–115.

Wang, J., Kim, S.C. and Pui, D.Y.H. (2008). Investigation of the Figure of Merit for Filters with a Single Nanofiber Layer on a Substrate. *J. Aerosol Sci.* 39: 323–334.

Wang, J. and Pui, D.Y.H. (2011). Characterization, Exposure Measurement and Control for Nanoscale Particles in Workplaces and on the Road. *J. Phys: Conf. Ser.* 304.

Wang, Z., Wagner, J. and Wall, S. (2011). Characterization of Laser Printer Nanoparticle and VOC Emissions, Formation Mechanisms, and Strategies to Reduce Airborne Exposures. *Aerosol Sci. Technol.* 45: 1060–1068.

Weimer, S., Mohr, C., Richter, R., Keller, J., Mohr, M., Prévôt, A.S.H. and Baltensperger, U. (2009). Mobile Measurements of Aerosol Number and Volume Size Distributions in an Alpine Valley: Influence of Traffic versus Wood Burning. *Atmos. Environ.* 43: 624–630.

Whitby, K.T. (1978). The Physical Characteristics of Sulfate Aerosols. *Atmos. Environ.* 12: 135–159.

Wu, C., Li, L. and Thornton, C. (2003). Rebound Behaviour of Spheres for Plastic Impacts. *Int. J. Impact Eng.* 28: 929–946.

Wu, C., Thornton, C. and Li, L. (2008). Rebound Behaviour of Spheres during Elastic-plastic Oblique Impacts. *Int. J. Mod. Phys. B* 22: 1095–1102.

Xu, M. and Willeke, K. (1993). Right-angle Impaction and Rebound of Particles. *J. Aerosol Sci.* 24: 19–30.

Yamada, S., Seto, T. and Otani, Y. (2011). Influence of Filter Inhomogeneity on Air Filtration of Nanoparticles. *Aerosol Air Qual. Res.* 11: 155–160.

Yin, Z., Lin, J. and Qian, L. (2012). An Experimental Study on the Characteristics of Nanoparticles Emission from a Vehicle. *Adv. Mater. Res.* 508: 180–183.

Yun, K.M., Hogan, J.r., CJ, Matsubayashi, Y., Kawabe, M., Iskandar, F. and Okuyama, K. (2007). Nanoparticle Filtration by Electrospun Polymer Fibers. *Chem. Eng. Sci.* 62: 4751–4759.

Received for review, July 15, 2013
Accepted, August 20, 2013